# Design of Control System for Constant Speed Variable Pitch Loaded Multi Axis Unmanned Aerial Vehicle Based on Lidar Technology

Xin Zhang(✉) and Mingfei Qu

College of Aeronautical Engineering, Beijing Polytechnic, Beijing 100176, China
zhangxin197802@163.com

**Abstract.** In order to ensure the stability of drone flight and improve control performance, a constant speed, variable pitch, and heavy-duty multi-axis drone control system design based on LiDAR technology is proposed. In the hardware design of the system, the power supply circuit for drone control is designed based on the principle of lithium battery charging and discharging circuit and the working principle of SX1308; Based on the mathematical model of drone position control, a control law for the horizontal position outer loop and the horizontal position inner loop was designed. Based on the closed-loop structure diagram of the drone position controller, a drone position controller was designed to ensure that the drone can accurately hover, return, and waypoint flight. In the software design of the system, LiDAR technology is used to extract drone trajectory features, and combined with drone control algorithm design, drone control is achieved. The system testing results show that the system in the article can achieve the expected design goals and improve the control accuracy to over 90%.

**Keywords:** laser radar technology · constant speed and variable pitch · multi axis UAV · control system

## 1 Introduction

By improving the load-bearing capacity of drones, larger scale cargo transportation and equipment carrying can be achieved, improving transportation efficiency and economic benefits. At the same time, by optimizing flight control algorithms and sensor integration, the stable flight of unmanned aerial vehicles in complex environments can be guaranteed, and the risk of accidents can be reduced. In addition, the design of the control system also involves enhancing autonomous navigation and task execution capabilities, enabling drones to autonomously plan paths, execute tasks, and make corresponding adjustments when encountering obstacles or faults [1]. This will reduce the burden of manual intervention, improve work efficiency and operational safety. From the above analysis, it can be seen that the research on the control system design of constant speed, variable pitch, and heavy-duty multi-axis unmanned aerial vehicles provides strong support for the widespread application of unmanned aerial vehicles in logistics, agriculture, rescue, and other fields, promoting sustainable development of society and economy.


L. Yun et al. (Eds.): ADHIP 2023, LNICST 548, pp. 148–161, 2024.
https://doi.org/10.1007/978-3-031-50546-1_10

In the above context, relevant scholars have proposed some system design methods. In order to improve the accuracy of agricultural unmanned aerial vehicle navigation, Wei Hongfei et al. [2] used sliding mode control method to establish a control model for navigation line tracking and master-slave system speed coordination, and verified the control effect of the controller through virtual simulation. The simulation results show that the use of sliding mode control method can effectively reduce navigation errors, allowing unmanned agricultural machinery to travel along the navigation line during operation with small centroid deviation. When sliding mode control method is used alone, there may be certain fluctuations in error, resulting in system instability. The introduction of PID feedback regulation control algorithm for further verification of the system indicates that the PID algorithm can effectively eliminate the fluctuation of system error, improve the stability of the system, and thereby improve the quality of agricultural machinery operation. Wu Yongcheng et al. [3] used Newton's law of motion and the law of rigid body rotation to establish the six degrees of freedom motion model of UAV, and obtained model parameters by means of experimental measurement and numerical simulation. The problem of control redundancy is solved by designing control Partition coefficient. The attitude controller based on linear active disturbance rejection control is designed, and its parameters are adjusted online by fuzzy control, which improves the response speed and robustness of the control system. Simulink simulation model is built, and the longitudinal flight control simulation test of UAV verifies the rationality of the designed control Partition coefficient and the effectiveness of the attitude controller. Yang K et al. [4] proposed a unmanned aerial vehicle control system based on Pixhawk flight controller, which consists of two subsystems: flight control system and spraying system. Using PX4 based firmware to implement Pixhawk flight control. The communication protocol is analyzed in detail, and the communication control between flight controller and spray controller is realized through serial port. The software part designs the remote control decoding task of the flight control system and the spray task of the spray system, realizes the communication between the flight control system and the spray system, and successfully completes the spray function. Shi Jia et al. put forward an improved design method for the control system of auto disturbance rejection quad rotor UAV. According to the actual parameters of the built quad rotor UAV, a numerical simulation model of the attitude control system of the quad rotor UAV was constructed. By comparing with the double closed-loop PID controller, it was proved that the designed Active disturbance rejection control system has strong anti-interference ability and high control efficiency under the premise of fast response and no overshoot.

Although the above methods can effectively control the flight of unmanned aerial vehicles, the control accuracy is relatively low. Therefore, this article applies LiDAR technology to the design of a constant speed, variable pitch, and heavy-duty multi-axis unmanned aerial vehicle control system. Lidar technology can provide high-precision environmental perception capabilities. By measuring the distance of the surrounding environment and the position of obstacles, real-time information about the terrain, buildings, and obstacles around drones can be obtained. This precise environmental perception helps drones avoid collisions, improve flight safety, and improve control accuracy.

## 2 Hardware Design of Control System for Constant Speed and Variable Pitch Loaded Multi Axis UAV

### 2.1 Design of Power Supply Circuit for UAV Control

The constant speed variable pitch loaded multi axis UAV is powered by batteries, and the power supply circuit is shown in Fig. 1.

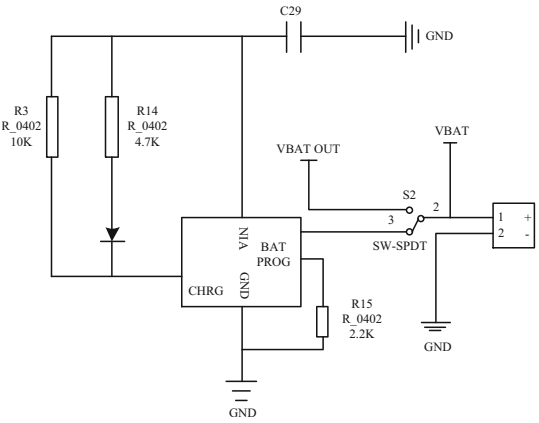


**Fig. 1.** Schematic diagram of lithium battery charging and discharging circuit

The figure shows the charging circuit of lithium battery. The chip is LTC4054, and pin 1 is the charge state pin. When the circuit is charged, the pin will be pulled down, and pin 1 is connected to the diode negative pole. When the lithium battery is discharged, the diode is lit, indicating that the battery is currently charging. Pin 3 is the charging current output pin, providing current and voltage. Pin 3 is externally connected to the lithium battery. Pin 5 is the standard pin of charging current. When connection point S2 contacts connection point S3, the lithium battery starts charging. When connection point S2 contacts connection point S1, the lithium battery supplies power to the system through VBAT-OUT.

In Fig. 1 the output voltage of Pin VBAT is 3.7 V, and the required voltage for system operation is 5 V. The chip SX1308 needs to increase the 3.7 V voltage to 5 V. SX1308 is a fixed frequency, SOT23-6 packaged current mode boost converter [5]. The operating frequency of up to 1.2 MHz allows smaller specifications of the external inductance and capacitance. The built-in soft start function reduces the starting impulse current. The working principle of SX1308 is shown in Fig. 2.

In Fig. 2, the output voltage is adjusted by the feedback voltage divider $R_1$ and $R_2$ to set the output voltage as:

$$VOUT = VREF \times (1 + \frac{R_1}{R_2}) \tag{1}$$

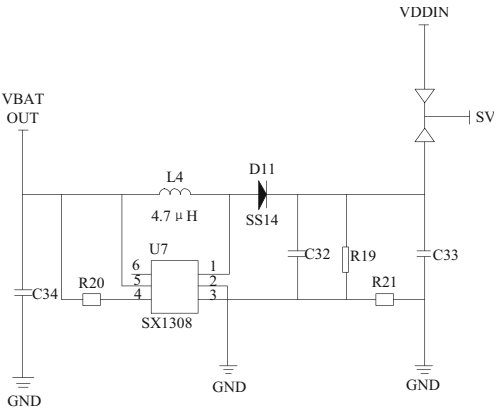


**Fig. 2.** SX1308 Working Principle Diagram

The chip SX1308 has 6 pins. SW is a switch node, which needs to be connected with inductance. GND is a grounding pin, FB is an output feedback pin, and the input feedback voltage is 0.6 V. EN is an energy pin. When the drive EN is greater than 1.5 V, it will activate, and when it is less than 0.4 V, it will stop. The EN pin cannot be suspended. In is an input power pin. The power supply voltage of the system chip is 3.3 V, and the 5 V voltage is reduced to 3.3 V through the voltage stabilizing chip XC6306.The voltage is detected by the voltage output pin VBAT_TST is connected to pin 10 of STM32, which has the function of ADC [6], and can be used to monitor the voltage of the system.

When using SX1308 chip, pay attention to the following in PCB layout:

- The input and output capacitors must be close to the GND pin of the IC to reduce the current loop area;
- AC current will flow through VIN, SW and VOUT cabling, so ensure that these cabling is short and wide;
- There is alternating voltage on the copper sheet at the SW pin. To prevent EMI, it needs to be controlled in a small area;
- The FB pin is a high impedance node. The FB wiring should be short enough to avoid noise causing output voltage fluctuations. The feedback resistor should be placed as close as possible to the IC. At the same time, R2 and GND should be placed as close as possible to the GND pin of the IC. The wiring from VOUT to R1 should be far away from inductance and switch nodes.

### 2.2 Design of UAV Position Controller

The position controller of UAV is designed to ensure that the UAV can perform position control functions such as hovering flight, homing flight and waypoint flight accurately, and it is also one of the necessary conditions for UAV to complete aerial photography tasks [7]. In the process of controller design, the difficulty of nonlinear controller design is often greater than that of linear controller design, so in order to achieve the design of position controller more easily, it is necessary to properly simplify and linearize the nonlinear mathematical model of UAV position control. According to the UAV position control mathematical model, it can be expressed as:

$$\begin{cases} \ddot{p}_x^e = -\frac{F}{m}(\sin\theta\cos\varphi\cos\psi + \sin\varphi\sin\psi) + f_x \\ \ddot{p}_y^e = -\frac{F}{m}(\sin\theta\cos\varphi\sin\psi - \sin\varphi\cos\psi) + f_y \\ \ddot{p}_z^e = -\frac{F}{m}\cos\theta\cos\varphi + g + f_z \end{cases} \tag{2}$$

Among them, $\varphi$, $\theta$ and $\psi$ represent the three channels of the UAV attitude, $f_x$, $f_y$ and $f_z$ represent the components of the three channels, $g$ represents the Gravitational acceleration, $m$ represents the UAV flight distance, and $F$ represents the resistance to the UAV flight.

From the above equations, it can be seen that the mathematical model of UAV flight control system is not a linear control system. In the process of position controller design, the introduction of nonlinear system should be avoided as far as possible, and it should be simplified. The position controller of UAV should be designed based on the simplified controlled object. If the UAV does not tilt at a large angle during flight, and the power generated by the blades on the boom is equal to the gravity of the UAV, the above nonlinear equation can be simplified as:

$$\begin{cases} \ddot{p}_x^e = -\frac{F}{m}(\theta\cos\psi + \varphi\sin\psi) + f_x \\ \ddot{p}_y^e = -\frac{F}{m}(\theta\sin\psi - \varphi\cos\psi) + f_y \\ \ddot{p}_z^e = -\frac{F}{m} + g + f_z \end{cases} \tag{3}$$

Finally, the plane rotation matrix constructed by heading angle $\psi$ can be decoupled into a linear model of three channels, namely, two horizontal channel position controllers and one altitude channel position controller.

For the above linear position model, the position of UAV horizontal channel and altitude channel can be obtained, and the kinematic model without disturbance can be obtained, which is expressed as:

$$\dot{p} = \begin{pmatrix} \frac{dp_x}{dt} \\ \frac{dp_y}{dt} \\ \frac{dp_z}{dt} \end{pmatrix} = \begin{pmatrix} v_x \\ v_y \\ v_z \end{pmatrix} \tag{4}$$

where, $p_x$, $p_y$ and $p_z$ are the three position channels in the horizontal and altitude directions respectively, and $v_x$, $v_y$ and $v_z$ are the three speed channels in the horizontal and altitude directions respectively. Formula (4) is a Kinematics model without any external interference, so the controller can control the UAV well, so the control law of the outer position loop can be designed as:

$$\vec{v}_{exp} = K_p\vec{e}_p \tag{5}$$

In the above equation, $\vec{v}_{\exp} = \begin{bmatrix} v_{x\_exp} & v_{y\_exp} & v_{z\_exp} \end{bmatrix}^T$ is the expected speed value, $\vec{e}_p = \begin{bmatrix} e_{px} & e_{py} & e_{pz} \end{bmatrix}^T$ is the outer loop error of the position controller, and $K_p$ is the adjustable parameter value of the proportional controller.

For the mathematical model of the controlled object in the position inner loop of UAV, it can be seen from Formula (3) that it contains unknown external disturbances, so the control law of the horizontal position inner loop can be designed as:

$$\begin{cases} \vec{e}_v = \vec{v}_{exp} - \vec{v} \\ \vec{u} = K_{pv}\vec{e}_v + K_{iv}\int_0^t \vec{e}_v dt \end{cases} \tag{6}$$

Among them, $K_{pv}$ represents the adjustable parameters of the proportional controller, $K_{iv}$ represents the adjustable parameters of the integral controller.

According to the above calculation, the closed loop structure block diagram of UAV position controller is designed, as shown in Fig. 3.

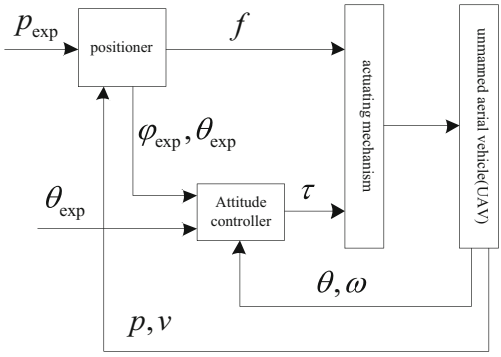


**Fig. 3.** Closed loop structure block diagram of UAV position controller

In conclusion, according to the internal and external loop control rate of horizontal position, the UAV position controller is designed.

## 3 Software Design of Control System for Constant Speed and Variable Pitch Loaded Multi Axis UAV

### 3.1 Extraction of UAV Track Characteristics

Using LiDAR technology to read drone trajectory image data from the CPU into the GPU, assuming $(x, y)$ represents the pixel coordinates of the drone trajectory image, $I(x, y)$ represents the original drone trajectory image, $\delta$ represents the scale coordinates of the drone trajectory image, and the Gaussian kernel calculation formula for the drone trajectory image is:

$$G(x, y, \delta) = \frac{1}{2\pi\delta^2} e^{-(x^2 y^2)/2\delta^2} \tag{7}$$

According to the above UAV trajectory image Gaussian kernel, the scale space of UAV trajectory image after filtering by Gaussian filter [8] is obtained, and the calculation formula is:

$$L(x, y, \delta) = G(x, y, \delta) * I(x, y) \tag{8}$$

On the basis of the above scale space, the Gaussian difference pyramid model of UAV trajectory image is constructed according to the UAV trajectory detected by the laser radar. The calculation formula is:

$$D(x, y, \delta) = L(x, y, \rho\delta) - L(x, y, \delta) \tag{9}$$

Among them, $\rho$ represents the scale coefficient of UAV trajectory image.

According to the Difference of Gaussians pyramid model $D(x, y, \delta)$ of the UAV trajectory image, remove the points and boundary points with low contrast, use the laser radar detection principle to determine the specific location of the UAV trajectory image feature points, use the Hessian matrix to calculate the Principal curvature of the UAV trajectory image, and judge whether the pixel $(x, y)$ in the model is a boundary point. The judgment formula is:

$$H = \begin{bmatrix} D_{xx} & D_{xy} \\ D_{xy} & D_{yy} \end{bmatrix} \tag{10}$$

Among them, $D_{xx}$, $D_{xy}$, $D_{yy}$ represents the partial derivative at the characteristic point of UAV trajectory image. Then we can get the trajectory and determinant value [9–11] of the Hessian matrix $tr(H)$ and $Det(H)$ representative, the calculation formula is:

$$tr(H) = D_{xx} + D_{xy} \tag{11}$$

$$Det(H) = D_{xx} \cdot D_{xy} - \left(D_{xy}\right)^2 \tag{12}$$

By setting a threshold $\psi$, if the following conditions are met, it is determined that the pixel is not a boundary point and is retained. On the contrary, it is determined that it is a boundary point and removed.

$$\frac{tr(H)^2}{Det(H)} < \frac{(\psi + 1)^2}{\psi} \tag{13}$$

On the basis of determining the feature points of the drone trajectory image, LiDAR technology is used to calculate the corresponding direction of the feature points, calculate the gradient amplitude and gradient directions $m(x, y)$ and $\mu(x, y)$ at feature point $(x, y)$ of the drone trajectory image, and generate the SIFT feature description vector of the drone trajectory image. The calculation formula is:

$$m(x, y) = \sqrt{\frac{(L(x + 1, y) - L(x - 1, y))^2}{+(L(x, y + 1) - L(x, y - 1))^2}} \tag{14}$$

$$\mu(x, y) = \arctan \frac{L(x + 1, y) - L(x - 1, y)}{L(x, y + 1) - L(x, y - 1)} \tag{15}$$

Read the UAV trajectory image data after Gaussian filtering from the CPU into the gpu, and construct the Gaussian difference pyramid model of UAV trajectory image using laser radar technology. The Hessian matrix calculates the constructed UAV trajectory

image Gaussian difference pyramid model in parallel in the gpu program, calculates the principal curvature of UAV trajectory image, and judges whether the pixels in the model are boundary points. Determine feature points and feature point gradient information, accumulate the obtained image feature point gradient information into gpu program, generate UAV trajectory image SIFT feature vector, and output it from CPU.

### 3.2 Design of UAV Control Algorithm

Assuming that $D_{sg}$ represents any reference point for the drone's flight, and an arc with a radius of $R$ is drawn towards the reference point, $L_{OI}$ represents the distance from the drone's current position to the reference point, $\eta_{sed}$ represents the angle between the line and airspeed $V$ between the drone's current position and the reference point, and $a_{afgh}$ represents the lateral acceleration that needs to be generated, then the distance from the drone's current flight position to the expected trajectory can be calculated using Formula (16):

$$Q_{aue} = \frac{L_{OI} \cdot V \times \eta_{sed}}{a_{afgh} \times D_{sg}} \times \frac{\{R\} + d_{dhk}}{cd_{zv}} \tag{16}$$

Among them, $d_{dhk}$ represents the weight of the UAV, $cd_{zv}$ represents the mass of UAV.

The acceleration command signal of the drone during flight is represented by $l_{zvj}$, and the lateral acceleration that needs to be generated is given using Formula (17):

$$a_{ag} = \frac{l_{zvj} + z_d}{k_{zbm}} \times p_{xn} \tag{17}$$

Among them, $z_d$ represents a viscous damped vibration system, $k_{zbm}$ represents a group of attitude angles of UAV in flight, $p_{xn}$ represents pitch angle.

$\lambda_{zhk}$ represents the dynamic range of the drone's pitch angle, while $h_{fhj}$ represents the real-time output of the three axis angular rate in the body coordinate system, satisfying the condition of $h_{fhj} = \left[h_{fhk}, h_{fhu}, h_{fhp}\right]$. Among them, $h_{fhk}$, $h_{fhu}$, and $h_{fhp}$ represent the angular velocities of each axis, then the expected roll angle command of the drone can be obtained using Formula (18):

$$E_{SG} = \frac{h_{fhj} + \left[h_{fhk}, h_{fhu}, h_{fhp}\right]}{\lambda_{zhk} + r_{sg} \times a_{ag}} - s_{sgj} \tag{18}$$

Among them, $a_{ag}$ represents the angle vector of geographical coordinate system, $r_{sg}$ represents the angular velocity information at the current time, $s_{sgj}$ represents the sampling time.

Assuming that $\omega_{sde}$ represents a single information fusion cycle, $l_{zbmk}$ represents the estimation of the drone's flight attitude at time $k$, and $l_{djh}$ represents the filter convergence criterion, the guidance law for drone flight attitude control is designed using Formula (19):

$$s_{sg} = \frac{l_{djh} \cdot l_{zbmk}}{\omega_{sde}} \times \frac{\left\{Q_{awe} + a_{ag}\right\}}{E_{SG}} \tag{19}$$

Assuming that $k_{sgj}$ represents the actual error of the filter, $\partial_{hp}$ represents the discrete state space of the UAV's lateral flight, and $l_{dhk}$ represents the statistical characteristics of each component of the UAV's lateral flight angle, then use Formula (20) to adjust the Natural frequency of the UAV guidance law:

$$W_{wet} = \frac{l_{dhk} \times \partial_{hp}}{k_{sgj}} \times s_{sg} \tag{20}$$

Assuming that $\tau_{dhk}$ represents the real-time collection of data for a special flight state dominated by lateral flight motion, Formula (21) is used to control the lateral flight attitude of the unmanned aerial vehicle:

$$f_{sh} = \frac{\tau_{dhk} \times W_{wet}}{E''_{SG}} \pm s_{sg} \tag{21}$$

To sum up, first calculate the distance from the current flight position of the UAV to the desired trajectory, give the required lateral acceleration, get the desired roll angle command of the UAV, design the attitude control guidance law [12–14] for the UAV's lateral flight, adjust the natural frequency of the unmanned mechanism guidance law, and complete the control of the UAV's flight attitude.

## 4 System Test Analysis

### 4.1 Experimental Platform

The experimental platform used in this paper is improved on the flight control system independently developed by the laboratory team.

The flight control system independently developed by the laboratory team takes GNSS and IMU module as the core. The whole flight control system includes the main control part (AP), IMU, geomagnetism (MAG), GNSS, data recording module (FDR), voltage converter (HUB) and signal light (LED). The details of each module are shown in Table 1.

For the improvement of the basic system, this paper mainly adds laser radar, visual camera and optical flow module. The laser radar used is RPLIDAR A1, which is common in 2D laser radar. The visual sensor used is Xiaomi binocular camera, with a resolution of 752 * 480 and a focal length of 2.1 mm. The output frame rate can be adjusted according to the actual use needs. In this application, the frame rate is set to 30 frames per second. The airborne computer adopts GIGABYTE of Gigabyte Technology, and its processor is Intel Core i7, with a size of 46.8 × one hundred and twelve point six × 119.4 mm.

Connect the laser radar and binocular camera to the airborne computer via USB, calculate the original data of the sensor through the computer to estimate the current moving distance, and send the calculation results to the AP through the serial assistant.

The hardware connection of the flight control system used in this paper is shown in Fig. 4.

**Table 1.** Basic Experimental Platform Module List

| Modular | Core components | major function |
|---|---|---|
| AP | STM32F407 | Complete the calculation of fusion and control algorithms, and convert the calculation results into PWM values of the motor |
| IMU | ICM20602 + MA5611 | Obtain real-time angular velocity and acceleration information of UAV |
| MAG | QMC5883 | Measuring the current magnetic field information of UAV for heading calculation |
| GNSS | NE06-M8N | Get the position and speed information of UAV in outdoor environment |
| FDR | HM-11 | Data recording module of UAV, integrated with Bluetooth module to set some parameters of UAV |
| HUB | TPS54560 | The voltage conversion module makes the UAV compatible with various types of batteries |
| LED | RGB | Set multiple flashing modes to reflect the health status of UAV |

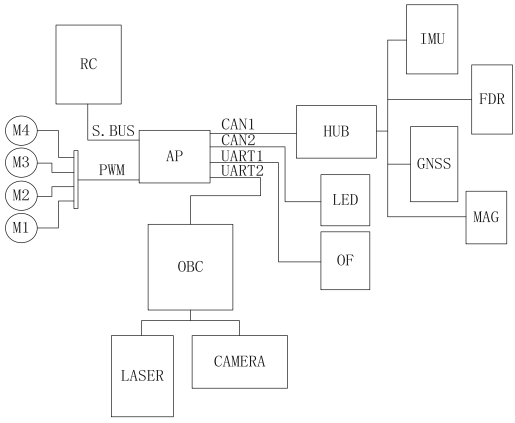


**Fig. 4.** Hardware Connection Diagram of UAV System

In addition, in order to obtain the real real-time position and speed information of UAV, this paper chooses to use a high-precision commercial RTK system, whose positioning error is within 0.05 m and speed error is within 0.1 m/s. The RTK system is placed on the UAV body, and the accuracy of the system in this paper is evaluated based on the comparison between the measured information and the results of the system in this paper.

The actual UAV used in this experiment is shown in Fig. 5.

**Fig. 5.** Physical picture of the experimental platform

### 4.2 Indoor Flight Test

For the indoor flight experiment, this paper selects an empty room as the flight experiment site. During the experiment, in order to ensure the normal operation of the laser radar and the visual camera, some cartons are arranged in the room as obstacles in advance.

The experimental process is: the UAV is operated by the pilot to fly slowly. The speed control mode is adopted during the flight. The speed target value of the given flight is operated by the remote controller, and the fused speed information is used as the real-time feedback value for speed control.

According to the above experimental scheme, the experimental results are as follows. In order to facilitate comparison, the position information measured by the positioning system has been transferred to the NED coordinate system in the flight control system.

Figure 6 shows the tracking of speed control during flight. The solid line in the figure is the target speed obtained by operating the remote controller, and the dotted line is the real-time speed of the merged UAV.

It can be seen from the figure that the response time of the speed control is about 2 s, which is faster than the speed control under the general GNSS environment and conforms to the characteristics of the designed system. The attitude angle comparison in the flight controller during flight is shown in Fig. 7.

Since the update frequency of attitude angle data is high, usually 400 Hz, the tracking delay of attitude angle tracking is lower than that of speed control tracking, and the angle tracking error is within $\pm 3°$.

According to the above results, the indoor flight error indicators are obtained, as shown in Table 2.

According to the analysis of the data in Table 2, the maximum error of attitude angle is 0.05 rad, and the existing scheme can achieve better attitude tracking effect. The maximum value of the speed error is 0.3, which is due to the delay of the designed speed control step response. When the speed tracking is stable, the error is kept within 0.1 m/s.

From the analysis of indoor flight results, it can be seen that the speed controller error of the system in this paper has been kept within 0.1 m/s, reaching the expected design goal.

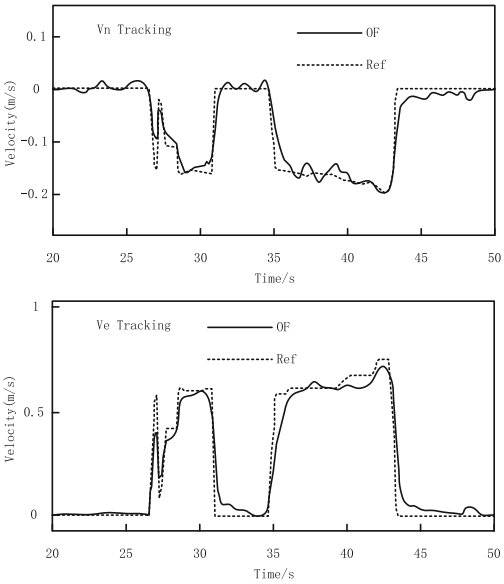


**Fig. 6.** Comparison of Indoor Flight Speed

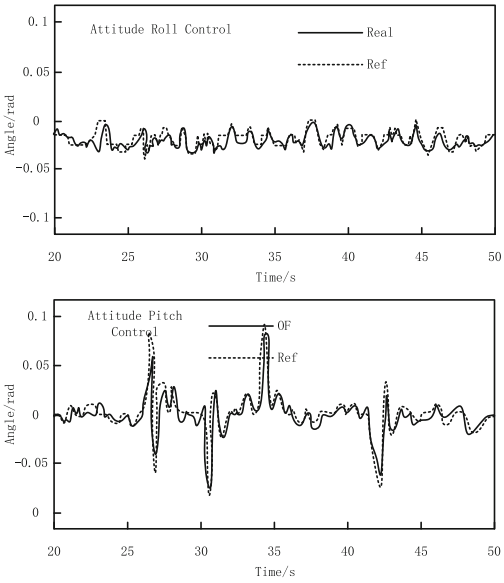


**Fig. 7.** Comparison of indoor flight attitude angle

### 4.3 Comparative Analysis

In order to avoid the singularity of the experimental results, the control system based on sliding mode controller, the control system based on fuzzy LADRC and the control

**Table 2.** Indoor Flight Error Indexes

| Reference indicators | Maximum | average value | standard deviation |
|---|---|---|---|
| Vn Err (m/s) | 0.07 | 0.0072 | 0.014 |
| Ve Err (m/s) | 0.31 | 0.023 | 0.049 |
| Roll Err (rad) | 0.029 | 0.002 | 0.004 |
| Pitch Err (rad) | 0.05 | 0.003 | 0.006 |

system based on Pixhawk - ScienceDirect are introduced for comparison, and the control accuracy of the constant speed and variable pitch loaded multi axis UAV is tested. The results are shown in Fig. 8.

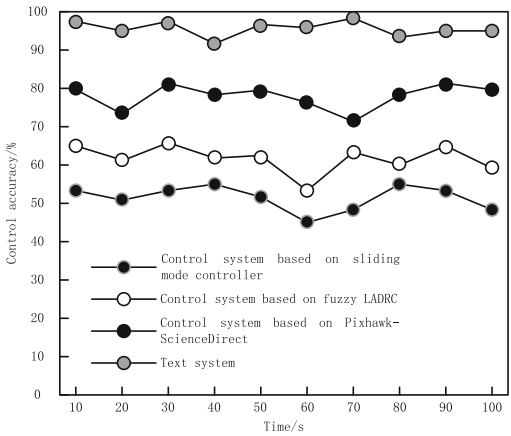


**Fig. 8.** Control Accuracy of Constant Speed Variable Pitch Loaded Multi axis UAV

It can be seen from the results in Fig. 8 that when the control system based on sliding mode controller and the control system based on fuzzy LADRC are adopted, the control accuracy of UAV is below 80%; When the control system based on Pixhawk - ScienceDirect is adopted, although the control accuracy of UAV is improved, it is still below 85%. When using the system in this paper, the control accuracy of UAV is more than 90%, which can ensure the stability of UAV flight.

## 5 Conclusion

This article proposes the design and research of a constant speed, variable pitch, and heavy-duty multi-axis unmanned aerial vehicle control system based on LiDAR technology. The results show that the system has high control accuracy, which can improve the control accuracy to over 90% and ensure stable flight of the unmanned aerial vehicle. Although this study has achieved certain results, there are still many shortcomings. In

the future, the focus will be on designing more efficient and stable control algorithms to achieve precise hovering, smooth takeoff and landing, and precise flight of unmanned aerial vehicles.

**Acknowledgement.** School level project of Beijing Polytechnic, Project Name: Research on Control System of Constant Speed and Variable Pitch Loaded Multi-axis UAV (2022X010-KXD).

## References

1. Feng, S., Li, Q.: Automatic navigation control system of agricultural UAV based on computer controller. J. Agricult. Mechaniz. Res. **44**(8), 42–46 (2022)
2. Wei, H.: Research on automatic navigation control system of agricultural UAV based on controller. J. Agricult. Mechaniz. Res. **44**(1), 218–222 (2022)
3. Wu, Y., Chen, Z., Su, L., et al.: Longitudinal attitude control of quad tilt-rotor UAV based on fuzzy LADRC. Flight Dynamics **38**(3), 28–33 (2020)
4. Yang, K., Yang, G.Y., Fu, S.: Research of control system for plant protection UAV based on Pixhawk - ScienceDirect. Procedia Comput. Sci. **166**, 371–375 (2020)
5. Shi, J., Pei, Z., Tang, Z., et al.: Design and realization of an improved active disturbance rejection quadrotor UAV control system. J. Beijing Univ. Aeronaut. Astronaut. **47**(09), 1823–1831 (2021)
6. Yao, H., Liu, Z., Zuo, H.: Research on control system of multi-functional UAV based on embedded system. J. Agricult. Mechaniz. Res. **44**(01), 142–145 (2022)
7. Pereira, L.G., Fernandez, P., Mourato, S., et al.: Quality control of outsourced LiDAR data acquired with a UAV: a case study. Remote Sens. **13**(3), 419 (2021)
8. Pang, Q., Wu, S., Niu, B., et al.: Design and implementation of micro air vehicle control system for IMAV 2019. Control Eng. China **28**(11), 2114–2122 (2021)
9. Zhu, H.: Design and experimental testing of safe flight control system for novel vertical take-off and landing aircraft. J. Vibroeng. **24**(3), 20 (2022)
10. Oh, D., Han, J.: Fisheye-based smart control system for autonomous UAV operation. Sensors (Basel, Switzerland) **20**(24), 7321 (2020)
11. Zhang, K., Bi, F.H., Li, K.L., et al.: Design and implementation of a dual-IP core UAV flight control system based on QSYS - ScienceDirect. Procedia Comput. Sci. **166**, 180–186 (2020)
12. Ding, D., Zhao, C., Jia, T.: Design of quadrotor unmanned aerial vehicle control system based on STM32. Mod. Electron. Techniq. **40**(01), 31–37+47 (2023)
13. Liu, G.: Application of genetic algorithm in plant protection UAV control system. J. Agricult. Mechaniz. Res. **45**(04), 221–224 (2023)
14. Qiu, J., Sun, Z.: RGPI observer-based control for wind disturbance rejection of quadrotor UAV. Comput. Simulat. **40**(01), 31–37+47 (2023)